Vibrational Spectroscopy 123 (2022) 103476

Contents lists available at ScienceDirect

Vibrational Spectroscopy

journal homepage: www.elsevier.com/locate/vibspec

Synchrotron FTIR investigations of kerogen from Proterozoic organic-walled eukaryotic microfossils.

C.C. Loron [a,b,*], MC Sforna [b], F. Borondics [c], C. Sandt [c], E.J. Javaux [b]

[a] Planetary Palaeobiology Group, UK Centre for Astrobiology, School of Physics and Astronomy, University of Edinburgh, Edinburgh, UK
[b] Early Life Traces & Evolution-Astrobiology, UR Astrobiology, University of Liège, Liège, Belgium
[c] SMIS Beamline, Synchrotron Soleil, Orme des Merisiers, 91190 Saint-Aubin, France

ARTICLE INFO

Keywords:
FTIR
Synchrotron FTIR
Organic-walled-microfossils
Precambrian
Kerogen
Raman

ABSTRACT

Fourier transform infrared spectroscopy (FTIR) provides a rapid non-destructive molecular characterization of organic and inorganic material in geological samples. Combination of qualitative and semi-quantitative approaches are routinely used in FTIR study of kerogen and coals. A diversity of descriptors provides straightforward tools to characterize kerogen type, composition and structure. However, only a few of these descriptors are applied in the chemical investigation of Precambrian organic-walled microfossils. Synchrotron radiation-based Fourier transform infrared microspectroscopy (SR-FTIR) permits high spatial resolution investigations of organic matter in a large range of applications in biology, geochemistry and cosmochemistry, but remains rarely applied in Precambrian microfossils studies. Here we show that SR-FTIR spectroscopy combined with an integrative approach of kerogen description is particularly relevant for the study of minute organic-walled microfossils of unknown biological origin. The analyses of five morphospecies from three different Proterozoic formations in northwestern Canada highlight kerogen signatures rich in aromatic, aliphatic and oxygenated moieties. This is evidenced by the combined use of spectrum qualitative descriptions (band assignments and positions) and the calculations of semi-quantitative parameters using intensities and integrated areas of absorption bands (CH_2/CH_3, $R_{3/2}$, Al/C═C, C═O/C═C, A factor, C factor). Altogether, this study demonstrates the interest of an integrative approach when investigating the chemistry of organic-walled microfossils with FTIR spectroscopy.

1. Introduction

The identification and characterization of extinct life forms is intrinsically linked to the identification of their chemical composition. Indeed, the preservation of organic remains and fossils in sediments is complex and depends on the interactions of biological and physico-chemical parameters [1], burial conditions and depositional environments but also significantly the original chemical composition of the organisms, the "precursor" effect. Studies of the transformations of various decay-resistant molecules through natural diagenetic processes and artificial taphonomy experiments have improved the understanding of the preservation potential of these molecules and of their source organisms [2–6].

Kerogen refers to the solid, insoluble, fraction of organic material that survives diagenetic processes and becomes stored in sedimentary rocks [7]. Organic-walled microfossils have a wall made of kerogen for which the molecular composition is derived from their original molecular composition modified by post-mortem decay and diagenesis processes. Because of its resistance, kerogen represents an inestimable archive of past microbial life that can be investigated using various molecular analytical approaches. In this regard, kerogen studies have strongly benefited from the development of spectroscopic instruments, including Raman and Fourier transform infrared (FTIR) spectroscopies (see [8,9]). IR spectroscopy allows a direct and rapid non-destructive profiling of organic material, its structure and its chemical composition. Its application to the chemical description of coal and kerogen (e.g., [10–15]) has provided great insights about the changes in organic matter occurring during degradation and maturation. In practice, FTIR investigations associate absorption bands in IR spectra to specific functional groups using reference spectra and literature. This approach

* Corresponding author at: Planetary Palaeobiology Group, UK Centre for Astrobiology, School of Physics and Astronomy, University of Edinburgh, Edinburgh, UK.
E-mail addresses: v1cloron@ed.ac.uk (C.C. Loron), mcsforna@uliege.be (M. Sforna), ferenc.borondics@synchrotron-soleil.fr (F. Borondics), christophe.sandt@synchrotron-soleil.fr (C. Sandt), ej.javaux@uliege.be (E.J. Javaux).

https://doi.org/10.1016/j.vibspec.2022.103476
Received 5 September 2022; Received in revised form 17 November 2022; Accepted 24 November 2022
Available online 25 November 2022

can be used to identify specific components within a kerogen but suffers from its very complex chemical structure, where many absorptions bands overlap [10,14]. The development of quantitative and semi-quantitative approaches, through deconvolution and fitting of spectral data, can help for the identification of functional groups but also provides interesting new tools for kerogen investigations. Proxies to quantify changes in aliphatic, aromatic and carbonyl/carboxyl groups, maturity index (aromaticity) and kerogen type were developed by many authors, sometimes with conflicting descriptors (see [14] and reference therein for review).

A diversity of parameters is used routinely for the investigations of kerogen (e.g., [10,13,14,16–20]). In the study of Precambrian (>542 Ma) organic remains, FTIR spectroscopy was mainly applied through assignments of specific absorption bands and their intensities (e.g. [21–25]). Very few studies have attempted a more integrative approach using a limited number of semi-quantitative parameters [8,26–30].

Analyses of microfossils in rock thin sections (e.g., [26,27,30,31]) are limited in the application of semi-quantitative calculation. Functional group absorptions of minerals, such as carbonate or silica, are known to vibrate at wavenumber similar to C-C, C-H bonds and carbonyl or ether groups within kerogen [30,32,33], leading to a superimposition of signals and a loss of exploitable information. To circumvent this problem, acid demineralization and extraction of the organic fraction is an efficient way to obtain isolated organic material on which to measure full infrared spectra without further altering the original signal [7,34].

Spectroscopic studies of organic microfossils must also consider the spatial heterogeneities observable within an individual. Differences of preservation or precursors between various zones of the same organism cannot be excluded [35] and study of such heterogeneities in specimens benefits from the use of high-resolution methods such as synchrotron-FTIR (SR-FTIR). Contrarily to traditional bench-top FTIR, SR-FTIR allows the detection of fine variations of absorption and acquisition of numerous spectra at a higher spectral and spatial resolution within the same object, notably thanks to a higher brightness of the source. SR-FTIR was successfully used in the study of microfossils in thin and ultra-thin sections [25,27,28] but its application has now to be extended on extracted organic-walled microfossils. This matters because affinities of Precambrian organic-walled microfossils are often unresolved, and the molecular characterization of their wall could provide great complementary information [20–24].

Semi-quantitative and qualitative parameters are applied here as an easy tool applicable for all FTIR study of Precambrian extracted organic fossils. In this study, they are used to describe the structure, composition and potential precursors of the kerogen from 5 morphospecies of organic-walled eukaryotic microfossils extracted from Precambrian shale rocks with SR-FTIR. Our findings demonstrate the usefulness of expanding classic integrative chemometric studies of kerogen to Precambrian biological remains.

2. Material and methods

2.1. Organic-walled microfossils

Morphologically complex organic-walled microfossils constitute interesting objects for spectroscopic investigation. In the Precambrian fossil record, especially before the Ediacaran, microfossil assemblages are dominated by unornamented taxa, i.e. leiospheres, that are probably polyphyletic [36–38]. The presence of complex morphological characters (complex ornamentation, processes) on a recalcitrant organic wall, on the other hand, permits to distinguish diverse eukaryotic morphotaxa that may belong to different biological species or life stages, and therefore may preserve distinctive and identifiable wall composition [22]. Chemometric approaches on such well identified morpho-groups is relevant to constrain and differentiate intra- and interspecific signals from maturity signals. Additionally, these approaches can also help constrain the original biological affinity of enigmatic microfossils (e.g., [22–24]). Here, we selected 5 morpho-species of organic-walled microfossils: *Germinosphaera bispinosa*, *Ourasphaira giraldae*, *Herisphaera triangula*, *Herisphaera arbovela*, and *Germinosphaera alveolata* (Fig. 1). The microfossils are all process-bearing (acanthomorphs) bearing either a single process (*G. bispinosa, G. alveolata*), that can branch (*O. giraldae*), or multiple processes, evenly distributed around the wall surface (*H. triangula, H. arbovela*). These microfossils were originally described and discussed in [24,39,40]. These microfossils are interpreted as being unambiguously eukaryotic based on the presence of large processes on their walls implying the presence of a complex cytoskeleton, a feature unknown in prokaryotes [41–43]. Although their precise taxonomical affiliation is unclear, it is probable that they represent protists, microalgae and fungi as suggested by their morphology and the molecular clock estimates for these groups [24,39,40].

The samples were all collected in northwestern Canada; in the Brock Inlier and Dismal Lakes area. Specimens of *Germinosphaera bispinosa*, *Ourasphaira giraldae* and *Herisphaera triangula* (Fig. 1) were extracted by acid demineralization from the shallow-water estuarine shale of the Grassy Bay Formation, lower Shaler Supergroup, Canada [39,44]. This formation is constrained between 1013 ± 25 Ma (U-Pb dating of detrical zircon) and 892 ± 13 Ma (Re-Os dating) [45–48]. *Herisphaera arbovela* specimens were extracted from lagoonal shale of the topmost Nelson Head Formation, lower Shaler Supergroup, dated by U-Pb dating of detrital zircon grains from fluvial quartz arenite at 1013 ± 25 Ma [45]. Finally, *Germiosphaera alveolata* specimens were extracted from shales of the Fort Confidence Formation, Dismal Lakes Group in Canada [40]. Fossiliferous samples hosting *G. alveolata* were dated at 1438 ± 8 Ma using Re–Os geochronology on crystalline pyrite [48]. Depositional setting of the Fort Confidence Formation is interpreted as shallow water with occasional aerial exposure [48]. All the microfossils are exceptionally well-preserved and belong to assemblages of great diversity [39,40].

2.2. Sample preparation

The microfossils are preserved as compressions less than 1 μm thick, parallel to lamination in shale (syngenetic). Their organic wall (the only cellular feature preserved) is made of kerogen and, therefore, the microfossils can be extracted from the rock matrix using acid maceration.

We used a procedure adapted from [49] that avoid mechanical manipulations and oxidation that could alter the kerogenous wall integrity and chemistry. We removed carbonate with hydrochloric acid (HCl, 35%) and silicate with hydrofluoric acid (HF, 60%). Hot HCl was used to remove neo-formed minerals. After neutralization of the acids with Milli-Q water, the microfossils were pipetted out of the macerate using an inverted microscope, deposited on ZnSe windows, and air-dried for at least 48 H before SR-FTIR analyses. We analyzed two specimens for each morpho-species.

No difference is observed in FTIR spectra of extracted kerogen after HF/HCL treatments [7,34]. HCL and to a lesser extent HF, have a hydrolyzing effect of organic matter but this effect is restrained to poorly evolved organic matter, such as in recent sediments, and negligeable in more evolved material [7]. Similarly, previous investigations on similar organic-walled microfossils have shown that no difference in Raman signal and calculated temperature were observed between specimens in rock sections and specimens extracted with the method above (e.g., [24,29,52]).

2.3. Synchrotron-FTIR spectroscopy

Infrared analyses were performed at the SMIS beamline at synchrotron Soleil (Saint Aubin, France). We collected the data using a Thermo Fisher Scientific Continuum FTIR microscope equipped with 32 × objective (0.65 numerical aperture) and matching condenser, a liquid-cooled narrow-band MCT detector, and coupled to a Nicolet 8700 spectrometer. For each specimen, background spectra were collected in

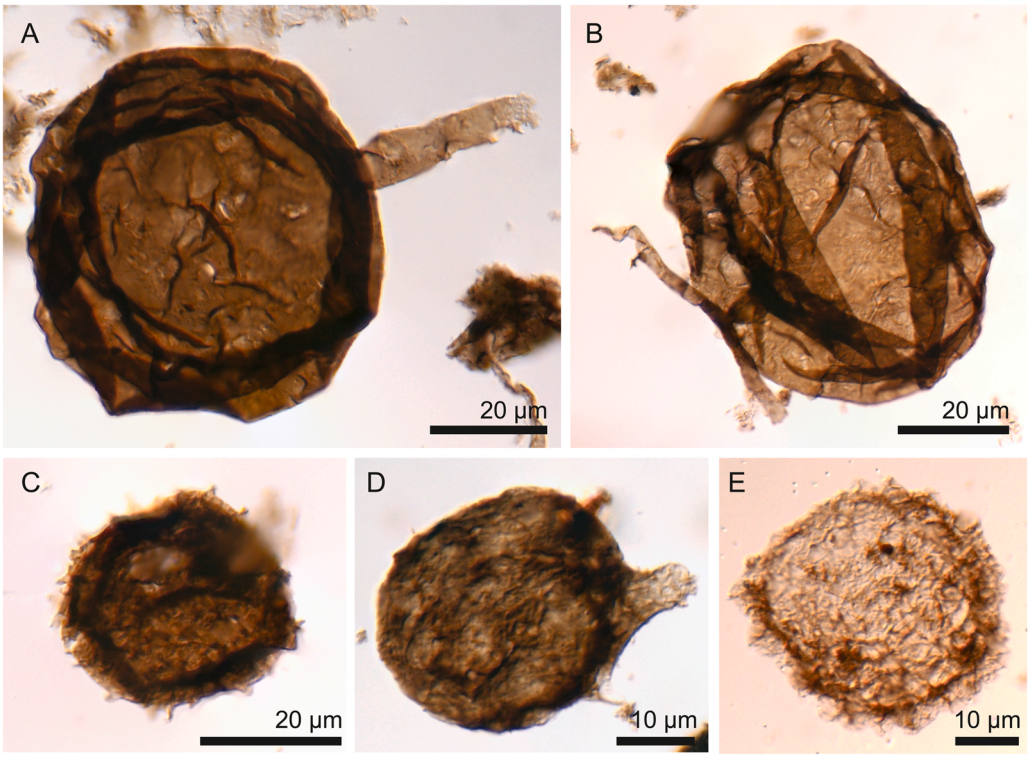

Fig. 1. Microphotographs of the studied morphospecies. *Germinosphaera bispinosa* (A); *Ourasphaira giraldae* (B); *Herisphaera triangula* (C); *Germinosphaera alveolata* (D); and *Herisphaera arbovela* (E). A-C are from Grassy Bay Formation and E from Nelson Head Formation, Shaler Supergroup, Canada [39]; D is from Fort Confidence Formation, Dismal Lakes Group, Canada [40].

the vicinity of the microfossil. 128 scans were accumulated in transmission mode at room temperature for each specimen (4000–650 cm^{-1}) with a spectral resolution of 4 cm^{-1}. The microscope was operated in the confocal (single-aperture dual-path) mode. The aperture was set to 10 × 10 μm^2 to obtain maps at a spatial resolution large enough to select representative spectra not affected by signals from surface artefact (e.g., amorphous fossil organic matter superimposed on the fossil surface) and experimental artefact (spectral distortion) while keeping the best possible signal/noise ratio. Spectral maps with a 5 µm step size were acquired for each specimen (Supplementary Fig. 1) on which we selected 3–5 representative spectra. Spectra were preprocessed using Omnic 9.2.41 (Thermo Scientific) and cut at 920 cm^{-1} to remove noise influence in the low wavenumbers. We applied Omnic automatic atmospheric correction to each spectrum. The spectra for each specimen were averaged resulting in 2 spectra by morphospecies (*G. bispinosa, O. giraldae, H. triangula, G. alveolata, H. arbovela*) and displayed on Fig. 2. Main regions of absorbance are shown in Table 1. Band assignments were made using literature [10,12,16,50,51] and with the help of the second derivative spectra (Savitzky-Golay filter with a window of 21; Fig. S2).

Spectra were deconvoluted in the C-H aliphatic region (ca. 3000–2800 cm^{-1}) and fitted following Painter et al. [10] and Lin and Ritz [12,16]. The ca. 1800–1500 cm^{-1} region was deconvoluted into two peaks: main peak of absorption for carbonyl/carboxyl C═O (centered at ca. 1700 cm^{-1}) and the main peak of absorption for aromatic C═C (centered at ca. 1600 cm^{-1}). Peak parameters such as area, width, and position were given by the software (Wire 4.0; Renishaw).

2.4. Raman geothermometry

The maximum temperature of burial for each sample was estimated using the Raman reflectance geothermometer described in Baludikay et al. [52]. Fossils investigated with SR-FTIR were then investigated by Raman spectroscopy at the University of Liège (Early life Traces & Evolution – Astrobiology Laboratory, Belgium). Raman spectra were collected using a Renishaw Invia Raman microspectrometer with an Ar-ion-100 mW monochromatic 514 nm laser source. Spectra were acquired in static mode fixed at 1150 cm^{-1}, allowing a 2000 cm^{-1} detection range and a 1 cm^{-1} spectral resolution. Beam centering and Raman spectra calibration were performed daily on a Si-glass with a characteristic Si-band at 520.4 cm^{-1}. The laser excitation was focused through a 100 × objective to obtain a 1–2 µm spot size. 15 spectra were acquired for each microfossil with a laser power of 1%, an integration time of 1 s and three acquisitions per spectra. Acquisitions were obtained with an 1800 l/mm grating illuminating a 1040 × 256 pixel CCD array detector. Spectra were processed with Wire 5.3® software (Renishaw). Data table and Raman spectra are displayed in Fig. S3 and Table 1. No spectra revealed residual mineral phases.

3. Semi-quantitative proxies

Several semi-quantitative proxies have been developed to help characterize kerogen (see Lis et al., 2005), including various calculation for aromatic, aliphatic and carbonyl moieties.

Painter et al. [10] separated the C–H aliphatic stretching region (ca. 3000–2800 cm^{-1}) into five bands; ~2955 and ~2865 cm^{-1} for CH_3 asymmetrical and symmetrical stretching, ~2925 and ~2850 cm^{-1} for CH_2 asymmetrical and symmetrical stretching, and ~2890 cm^{-1} for CH stretching. This approach was subsequently used in other studies (e.g., [10,12,16,53]. Lin and Ritz [12,16] use the integrated area intensities of band in the CHx stretching region (ca. 2800–3000 cm^{-1}; although calling it integrated intensity ratio) to estimate the relative concentration in terminal CH_3 and methylene CH_2, reflecting aliphatic chain length and degree of branching (eq1). For such calculation, bands for asymmetric stretching of CH_2 and CH_3 are considered diagnostic [10,12,16], as deconvolution of close absorption bands (symmetric stretching bands of CH_2 and CH_3) is difficult and misleading [12,16,53]. Most following studies (e.g., [8,13,30,1729]) calculated CH_2/CH_3 ratio by using peak

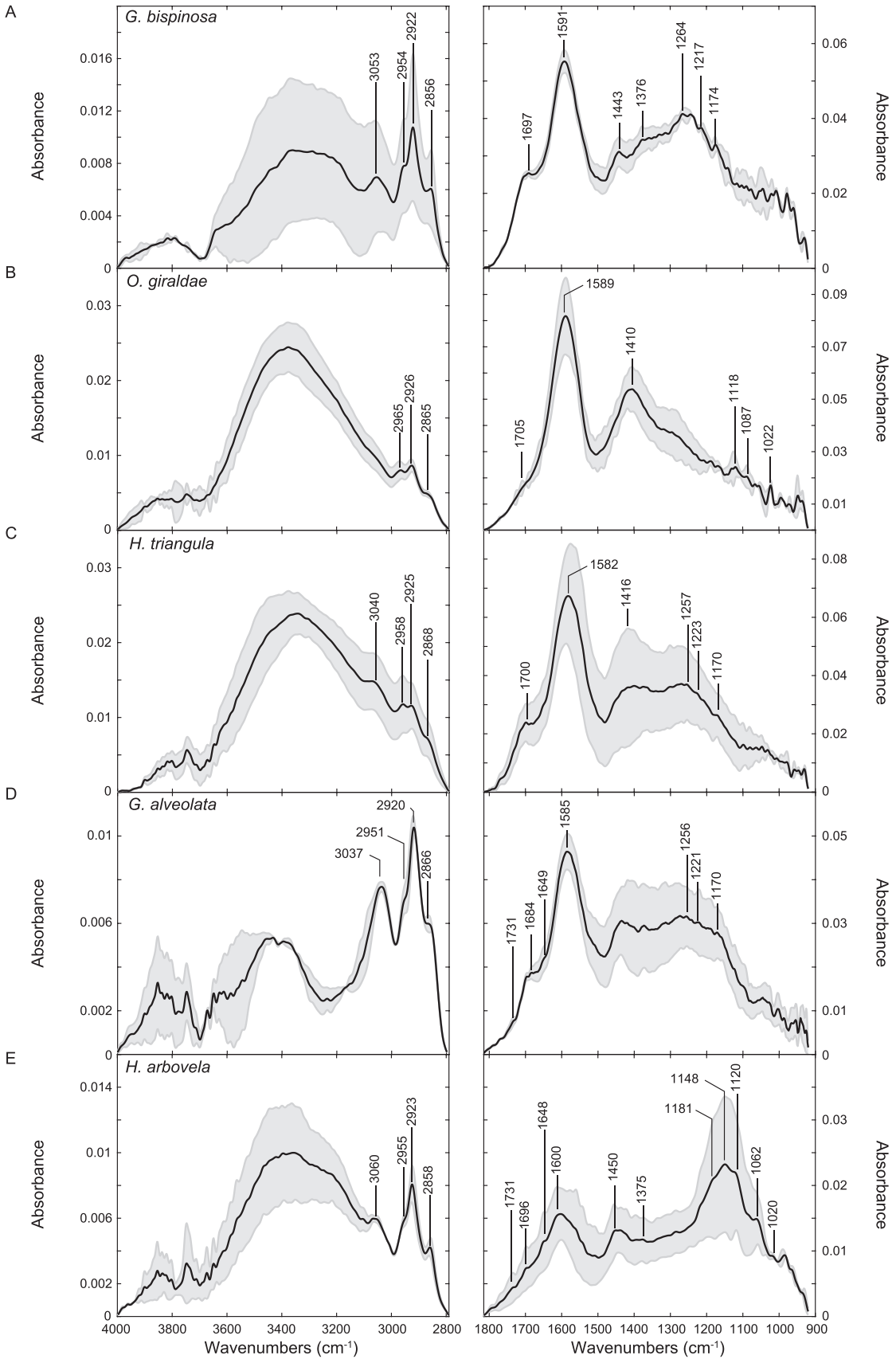

Fig. 2. Non-normalized representative spectra for *G. bispinosa* (A); *O. giraldae* (B); *H. triangula* (C); *G. alveolata* (D); and *H. arbovela* (E). Marked bands are discussed in the text. Black lines represent average spectra for two specimens of each morpho-species. Gray areas represent full variability between these two specimens.

Table 1
FTIR band assignments.

Wavenumber (cm^{-1})	Assignments[10,12,16,50,51,56]
3400–3320	OH stretching, NH stretching
3080–3010	Aromatic CH stretching, NH stretching
3000–2800	Aliphatic CH stretching
1800–1650	Carbonyl/carboxyl C═O stretching
1625–1500	Aromatic C═C stretching, carboxylate
1480–1330	Aliphatic CHx deformation, carboxylate
1225–1200	Aromatic ether C-O-C, Phenol CO
1200–970	Aliphatic ether C-O-C, alcohol CO, CO/CC stretching

intensity (height) and not area under each peak as proposed by Lin and Ritz, p. 270 in [16]: "With the use of integrated band areas for the CH2 and CH3 asymmetric stretching vibration […]".

$$CH_2/CH_3 = \frac{A_{asCH_2}}{A_{asCH_3}} \quad (1)$$

Igisu et al. [54], and further studies [25–28,31,55], use the $R_{3/2}$ ratio (eq2) as an indicator for aliphatic chain length/degree of branching. This ratio uses the peak height (intensity) of asymmetrical stretching peaks for CH_2 and CH_3 and was proposed as a proxy for establishing biological affinities of micro-organisms to eukaryotes, bacteria or archaea, notably based on differences of carbon chain length of their lipids.

$$R_{3/2} = \frac{I_{asCH_3}}{I_{asCH_2}} \quad (2)$$

Methods by Lin and Ritz [12,16] and by Igisu et al. ([54]; and further studies) allow conversion of the CH_2/CH_3 and $R_{3/2}$ ratio into carbon number of the n-alkane chain.

During maturation, a shortening of aliphatic chains occurs, due to the lower energy required to break α-β carbon bonds in comparison to other C-C bonds. This breaking results into a decrease of the observed CH_2/CH_3 ratio [12,14] or an increase in the $R_{3/2}$ ratio [54]. Similarly, the removal of oxygen-bearing functions during diagenesis and maturation results in a decrease of detectable C═O groups (although some carbonyl, carboxyl and ester groups might appear during the early diagenesis from fossilization products of sugars and protein [56,57] and from interaction with the mineral matrix [58]). Nevertheless, in earlier diagenetic stages, preservation of original components within resistant cell wall of microorganisms is not precluded. Coatings of resistant material within wall and rearrangement of aliphatic chains during diagenesis provide a shelter for less resistant compounds [4,34]. A rapid deposition in clay minerals, partly linked to the inhibition of environmental decomposers [2,59,60], might also favor the long-term detection of biopolymer signals in microfossils, although modified by the diagenetic processes.

These changes of state during maturation can be expressed using chemometric parameters. Aliphatic C-H/aromatic ratio (Al/C═C) illustrates the relative abundance of aliphatic to that of aromatic whereas carbonyl/aromatic ratio (C═O/C═C) show the evolution of carbonyl/carboxyl groups contribution relative to aromatic groups [10,14,18,19]. Al/C═C and C═O/C═C ratios typically decrease with increasing maturity [14,61].

Using the integrated areas of these peaks, we can calculate Al/C═C (eq3) and C═O/C═C ratio (eq4). In eq3, A(3000–2800) corresponds to the integrated area of the whole aliphatic region (3000–2800 cm^{-1}) and A(~1600) corresponds to the integrated area of the aromatic band at ca. 1600 cm^{-1}.

$$Al/C = C = \frac{A_{(3000-2800)}}{A_{(\sim 1600)}} \quad (3)$$

$$C = O/C = C = \frac{A_{(1800-1600)}}{A_{(\sim 1600)}} \quad (4)$$

In 1987, Ganz and Kalkreuth [11] introduced the A and C factor. A factor indicates the changes in intensity of the aliphatic groups and C factor represent the changes in the C═O groups. Both factors are influenced by thermal maturity and changes observed between the different material from different assemblages may be due to different precursors, preservation and burial conditions [3,11,20].

Furthermore, these parameters can be used in an A factor vs C factor diagram, in an equivalent of the H/C-O/C van Krevelen diagram [11,13,19], giving the type of kerogen (among type I, II, III) of the studied specimens.

Following Ganz and Kalkreuth [11] and subsequent works [13,14,18–20], we can calculate A factor (eq5) and C factor (eq6) for each of our specimens using integrated band areas of aliphatic region (3000–2800 cm^{-1}); aromatic peak (ca. 1600 cm^{-1}) and C═O peak (ca. 1700 cm^{-1}) in order to track the changes in relative intensity of the aliphatic groups and in carbonyl C═O groups.

$$Afactor = \frac{A_{Al}}{(A_{Al} + A_{C=C})} = \frac{A_{(3000-2800)}}{(A_{(3000-2800)} + A_{(\sim 1600)})} \quad (5)$$

$$Cfactor = \frac{A_{C=O}}{(A_{C=O} + A_{C=C})} = \frac{A_{(\sim 1700)}}{(A_{(\sim 1700)} + A_{(\sim 1600)})} \quad (6)$$

All these parameters are considered semi-quantitative because they do not represent the total amount of each of their descriptors but only their main spectral fraction. The spectral and molecular complexity of kerogen precludes the direct application of quantitative parameters, especially in region where band overlaps is common (e.g., from 1800 cm^{-1} and below). Average values obtained for each parameter and for each microfossil are shown on Figs. 2–4.

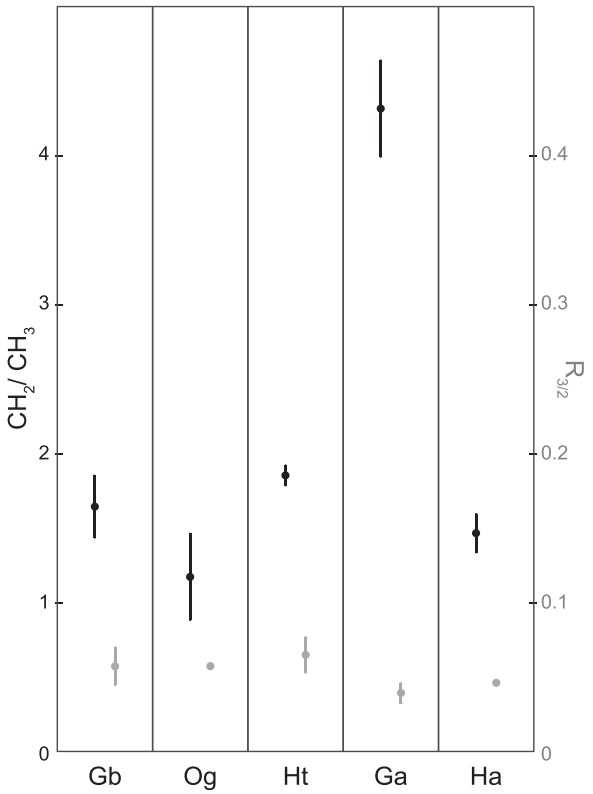

Fig. 3. Aliphaticity indexes. (Gb) *G. bispinosa*. (Og) *O. giraldae*. (Ht) *H. triangula*. (Ga) *G. alveolata*. (Ha) *H. arbovela*. Axes represent on the left CH_2/CH_3 ratio [12,16] and on the right $R_{3/2}$ [54].

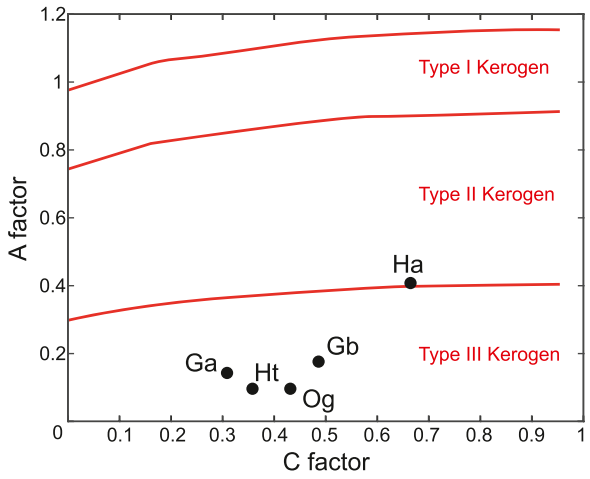

Fig. 4. A and C factors. (Gb) *G. bispinosa*. (Og) *O. giraldae*. (Ht) *H. triangula*. (Ga) *G. alveolata*. (Ha) *H. arbovela*.
The graph type is adapted from [13] and [19].

4. Results

4.1. Raman spectroscopy

The investigation of the fossils by Raman spectroscopy shows Raman spectra (Supplementary File) with an intensity of D1 lower than G; a large D1 band (FWHM < ~150 cm^{-1}) and well-developed D3 and D4 bands. Such features are indicative of a rather poorly ordered carbonaceous material [62–64]. The maximal temperatures that these fossils underwent during burial are comprised between 120 °C and 180 °C, consistent with previous investigations of similar material [24] and regional metamorphism [44,64]. These differences can be explained by different sampling location and in a same formation by difference in the precursor [52,65]. Overall, the maximum temperature of burial is compatible with preservation of primary signals within the kerogen forming the microfossils.

4.2. Qualitative observations

Qualitative investigation of micro-FTIR spectra for each of the microfossils unravels similar general absorption characteristics, indicating the presence of similar functional groups typical of kerogen (Table 1; Fig. 2).

We observe a broad intense band centered around 3400 cm^{-1} for each specimen attributed to various hydroxyl compounds vibrations (OH stretch; due to the small thickness (~1 μm) and considering the drying of the specimen, it is unlikely that they result from liquid water) and NH stretch [50]. The spectra show a weak to moderate absorption band between 3046 and 3060 cm^{-1}. A band at this wavenumber in kerogen is usually attributed to aromatic C-H stretching of unsaturated (C═C-H) and aromatic ring [10,50] but, at low burial temperature, might also represent vibration of NH bond (Amide A/B) and N-moieties from fossilization products of sugar and protein polymerization [56]. Distinct characteristic bands, assigned to aliphatic C-H vibrations are also observed for all specimens. These bands include asymmetric stretching of methylene (CH_2) and methyl (CH_3) around 2925 and 2960 cm^{-1}, respectively; and symmetric stretching of CH_2 at ~2855 cm^{-1}. Additional absorption bands of symmetric CH_3 and CH can be found in this region but require specific deconvolution [10,12,16].

An absorption band is present around 1700 cm^{-1} for all the microfossils. In kerogen, bands centered around 1700 cm^{-1} can be attributed to carbonyl stretching (C═O) of carboxylic acid, quinone, ketone or aldehyde [10,15,19,33,50] resulting from cellular precursors and peroxidation products of sugar and protein material during fossilization.

A broad intense absorption centered at 1582–1600 cm^{-1} in kerogen, present in all microfossils spectra here, would result mainly from the contribution of polyaromatic structures, resulting from carbonization of the organic material with possible subordinate absorption of alkene, conjugated carbonyl, carboxylate and amide groups [10,19,50,51,66,67]. This band absorption is often enhanced by the presence of oxygenated moieties linking the aromatic rings (e.g., ether bridges; [10]) explaining its strong intensity despite the smaller dipolar moment of carbon-carbon bonds compare to oxygenated groups [10]. Therefore, despite these differences in absorptivity, this band can still be retained for representing aromatic moieties in semi-quantitative parameter. In addition to the polyaromatic absorption around 1590 cm^{-1}, weak absorptions observed on the second derivative (see Supplementary Fig. 1) between 1498 and 1510 cm^{-1} in all microfossils are possibly due to the vibration of single aromatic ring [3,10,17].

Absorptions of various intensities in the region 1480–1330 cm^{-1} are present in all specimens, due to various CH_x deformation. Bands at lower wavenumbers, in the 1350–970 cm^{-1} region, have a poorly defined and complex character which make difficult assignment to specific functional groups [10,14]. This region mainly record absorption from phenol and ether compounds [50,51]. C-O from phenol and alcohol show absorption between 1260 and 1000 cm^{-1}.

Absorption centered between 1150 and 1085 cm^{-1} (often around 1125 cm^{-1}) is characteristic of asymmetric C-O-C stretching in aliphatic ethers [51]. This absorption is observed in similar range for acyclic and 6 atom cyclic ethers. Between 1200 and 970 cm^{-1} we also observed various absorptions for C-O and C-C stretching. Stretching mode of C-O are usually coupled with vibration of adjacent C-C bonds [50,51].

The main differences between microfossil species foremost reside in differences in relative absorption intensities. Spectra from *G. alveolata* (Fig. 2C) present stronger absorption at 3040 cm^{-1} than the other fossils, probably due to the higher aromatic contribution in addition to the stretching NH at this wavenumber. Vibrations of carbonyl C═O centered around 1730 cm^{-1}, present as shoulder in *G. alveolata* and *H. arbovela* are typical of C═O stretching in esters [30,33,50].

In *H. alveolata* and *H. arbovela*, the absorption at 1648 cm^{-1} (Figs. 2D, 2E) can be interpreted as C═O stretching in amide [50] as observed in low temperature melanoidins [56] and corresponding to fossilization products of the original protein/sugar moieties.

Bands attributed to phenol are observable in *G. bispinosa* (1264; 1217, 1174 cm^{-1}) and more discretely in *H. triangula* (1257; 1223; 1170 cm^{-1}) and *G. alveolata* (1256; 1221; 1170 cm^{-1}) (Fig. 2A, C, D). Bands that could represent combination bands of phenol between 2000 and 1660 cm^{-1} [51] are observed on the second derivative (Supplementary Fig. 2), although with a very weak absorption.

O. giraldae and *H. arbovela* (Fig. 2B, E) present an absorption between 1150 and 970 cm^{-1} that could reflect a contribution of remaining saccharidic content as this is a highly specific region for carbohydrate in living organisms [68,69,71]. In *H. arbovela* (Fig. 2E), the absorption in this region is the highest contribution of the whole spectrum with a broad triplet of bands at 1120, 1148 and 1181 cm^{-1}, in addition to bands at 1062 and 1020 cm^{-1}. However, pristine polysaccharide absorption shows maxima between 970 and 1100 cm^{-1} [67,70,71]. This is not the case in *O. giraldae* and *H. arbovela* that show a maximum at 1118 and 1148 cm^{-1}, respectively (Figs. 2B, 2E). Therefore, the absorption in the 1150–970 cm^{-1} interval might result from ether moieties derived from fossilization reactions of original organic precursors, possibly carbohydrate, but not from directly preserved sugar content. In addition, in *G. alveolata* and *H. arbovela*, which both present an absorption band from ester around 1730 cm^{-1}, it is also probable that C-O stretching from lipid esters [51] partly contribute to the absorption in the interval 1300 – 1100 cm^{-1}, in coherence with the high CH stretching absorption.

Small differences can also be observed between specimens from the same species (Fig. 2; Fig. S2), resulting from preservation intra-specific heterogeneities, but with no alteration of the general signal. These heterogeneities mainly include difference in intensity. In one specimen

of *H. triangula* a band is present around 1416 cm^{-1}, which is not recorded on the second specimen. A band around this wavenumber is also observed in *Ourasphaira* and might be due to the combination of various smaller absorption bands vibrating in this region (e.g., CH in plane deformations and carboxylate; [50]). In one specimen of *H. arbovela*, the band at 1600 cm^{-1} represents the sum of two main absorption at 1611 (aromatic C═C stretching) and 1565 cm^{-1} (carboxylate). It illustrates why kerogen infrared studies are most often limited to semi-quantitative parameters [14].

4.3. Semi-quantitative analysis

The calculation of aliphaticity indexes yields large differences between specimens depending on the methods of calculation (Fig. 3; Table 2). Calculations following Igisu and colleagues' method ([54] and subsequent work) discriminate the specimens from Grassy Bay (0.57–0.65) from the other microfossils (0.39 and 0.46) whereas with Lin and Ritz's method, the results are more scattered. Using the charts presented in Lin and Ritz ([16]; fig. 6) we can estimate the number of carbon atoms by chain at ca. 12 for *Germinosphaera alveolata;* ca. 10 for *Germinosphaera bispinosa* and *Herisphaera triangula;* and ca. 8 for *O. giraldae* and *H. arbovela*. Using the chart in Igisu et al. ([54]; fig. 6) we can estimate these numbers at 9–10 for *G. bispinosa*, *O. giraldae* and *H. triangula;* and ca. 15–16 for *H. arbovela* and 18 for *G. alveolata*.

Specimens with high A and C factors (*H. arbovela*) show a molecular structure rich in aliphatic and oxygenated compounds. Higher A factor associated with low C factor, as observed for *G.alveolata* suggest a growing influence of aliphatic moieties over oxygenated groups. *G. bispinosa* C value illustrates a contribution of oxygenated groups coupled with moderate aliphatic influence. *O. giraldae* and *H. triangula* present a higher contribution of oxygenated moieties over aliphatic ones. Calculated A and C factors for each microfossil can be plotted on a diagram equivalent to van Krevelen H/C vs O/C plot (Fig. 4) [11,13,19], showing the similarities of the different morpho-species to the various kerogen types. The microfossils are plotted in the type III kerogen region except for *H. arbovela* (Type II).

High value for Al/C═C ratio (Fig. 5A) are observed for *Herisphaera arbovela* (0.71) and indicates of an enrichment in aliphatic moieties. The specimens from Grassy Bay and *G. alveolata* on the other hand show lower values (0.11–0.22). This ratio typically decreases with thermal maturity, reflecting the aromatization and graphitization of the organic material (e.g., [14,73–75]), suggesting that these microfossils are more mature.

Specimens of *Germinosphaera bispinosa* and *Herisphaera arbovela* present the highest C═O/C═C values (0.95 and 1.99, respectively) (Fig. 5B), and therefore a higher contribution of carbonyl/carboxyl signals, whereas other microfossils present more moderate (*O. giraldae,* 0.77) or lower values (*H. triangula (*0.58), *G. alveolata* (0.45)). The variations observed between all the specimens suggests that the results for this parameter are decorrelated from preservation conditions.

5. Discussion

The plotting of the microfossils on the A factor vs C factor diagram (Fig. 4) in the type III domain (*G. bispinosa, G. alveolata, H. triangula, O. giraldae*) and type II domain (*H. arbovela*) reveals the inherent difficulty of interpreting IR spectroscopic data from material of unknown or unclear biological origin. Precursors of type III kerogen are usually plant based, made of degraded lignin and cellulose products whereas Type II, with a higher aliphatic contribution, may be algal in origin [4]. The present microfossils are evidently too old to be originated from plants, but this plotting suggests that they share chemical similarity in their precursors. For example, lignin is a condensed polymer of cross-linked paracoumaryl, conyferyl and sinapyl alcohol and we observed functional groups in common with these molecules in our microfossils (e.g., phenol, aromatic ring, alkene). The various alterations and destructions

Table 2
Semi-quantitative ratio values.

	parameter	Al	C═C	C═O	CH_2/CH_3	$R_{3/2}$	Al/ C═C	C═O/ C═C	A' factor	C' factor	averages					
											CH_2/CH_3	$R_{3/2}$	Al/ C═C	C═O/ C═C	A' factor	C' factor
	wavenumber	3000–2800 cm^{-1}	~1600 cm^{-1}	~1700 cm^{-1}												
Microfossils	specimen #	area	area	area	area	intensity										
Germinosphaera bispinosa	**b1 germ6**	1.20	4.07	3.81	1.43	0.44	0.30	0.93	0.23	0.48	1.64	0.57	0.22	0.95	0.18	0.49
	b1 germ8	0.54	3.82	3.68	1.85	0.70	0.14	0.96	0.12	0.49						
Ourasphaira giraldae	**b1 oura2**	0.63	5.03	4.66	0.88	0.56	0.13	0.93	0.11	0.48	1.17	0.57	0.11	0.77	0.10	0.43
	b2 oura1	0.60	6.93	4.30	1.46	0.59	0.09	0.62	0.08	0.38						
Herisphaera triangula	**b2 heri7**	0.64	8.08	3.32	1.92	0.77	0.08	0.41	0.07	0.29	1.85	0.65	0.11	0.58	0.10	0.36
	b2 heri8	0.60	4.46	3.31	1.78	0.53	0.13	0.74	0.12	0.43						
Germinosphaera alveolata	**b3 germ8**	0.57	3.57	1.50	3.99	0.32	0.16	0.42	0.14	0.30	4.31	0.39	0.17	0.45	0.15	0.31
	b3 germ9	0.67	3.71	1.75	4.64	0.46	0.18	0.47	0.15	0.32						
Herisphaera arbovela	**b4 heri7**	0.78	1.48	3.10	1.59	0.47	0.53	2.10	0.35	0.68	1.46	0.46	0.71	1.99	0.41	0.67
	b4 heri8	0.56	0.63	1.19	1.33	0.45	0.88	1.88	0.47	0.65						

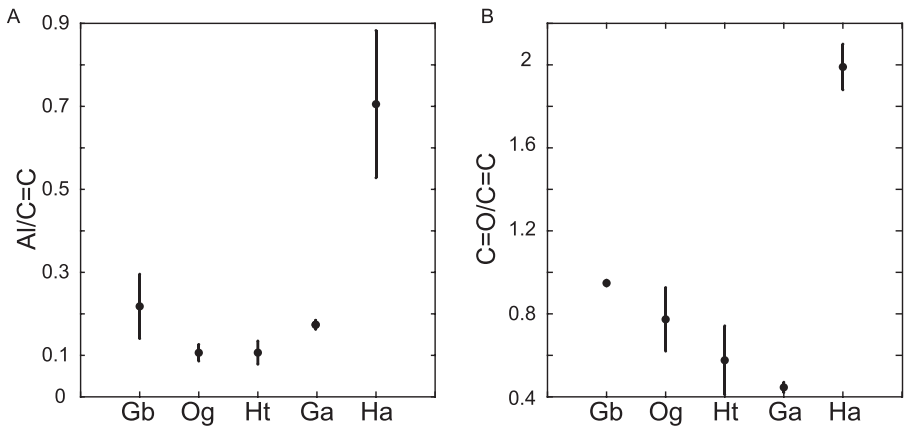

Fig. 5. Semi Quantitative parameters. A) Aliphatic/aromatic ratio. B) Carbonyl/aromatic ratio. On the x axis: (Gb) *G. bispinosa*. (Og) *O. giraldae*. (Ht) *H. triangula*. (Ga) *G. alveolata*. (Ha) *H. arbovela*.

occurring before and during diagenesis are often difficult to track on isolated material in addition to be still not fully understood [4]. Because of the numerous convergences in chemical functions and the molecular structural complexity of kerogens, qualitative or semi-quantitative proxies on their own have little weight. Therefore, the combination of chemometric approaches is particularly relevant when investigating FTIR data on unknown objects [14].

A vibrant example concern aliphaticity proxies. Lipids and other long-chained structural compound (e.g., algaenan) are amongst the most resistant molecules to degradation [4,34], so to find long aliphatic chains in very old organic microfossils is not precluded. To obtain information on chain length or degree of branching, this observation must be supported by semi-quantitative calculation following various established methods [12,16,54]. Author interpretations on applications of semi-quantitative parameters have also to be considered, as it has been noted before (see Section 3). Our calculations following the two methods lead to diverging results (Fig. 3), especially for *G. alveolata* and *H. arbovela*. The two methods have their pros and cons. Using peak intensities might lead to an overestimation of the ratios (highest point of the peak affected by noise) whereas using area might lead to an underestimation (averaging at lower value) but will be less susceptible to noise. In our case, this is what is observed with *G. alveolata* and *H. arbovela* values using Lin and Ritz's method (area). Values obtain with Igisu's method are more coherent with the qualitative observation of the spectra and are retained here for discussion.

In FTIR spectra, main absorption bands for saccharides are usually observed between 1200 and 800 cm^{-1} (absorption of CO, CC, C-O-C bonds), with a maximum absorption around 1030–1050 cm^{-1} [68,71,72]. *Herisphaera arbovela* high absorption in this region (Fig. 2E and Supplementary Fig. 2) could suggest an original composition richer in polysaccharides but the main absorption in our microfossils is rather represented by a band at 1150 cm^{-1}. An increase of absorption at this wavenumber is observed at very high temperature, corresponding to bonds formed between aromatic structures [76]. However, the low aromaticity observed in *H. arbovela*, the high aliphaticity and the low calculated Raman temperature of ~120 °C, rather suggests that the absorption observed in the interval 1200–1000 cm^{-1} reflect original precursor, modified through diagenesis, such as fossilization products of sugars-proteins [56] or fatty acids [51]. Similarly, specimens of *G. bispinosa*, *O. giraldae* and *H. triangula* from Grassy Bay Formation have undergone similar burial conditions and their variations certainly reflect differences in their original composition. This is supported by the minor differences observed in the Raman spectra for these three fossils coming from the same locality.

The taxa studied here have been interpreted as probable microalgae, protists, or fungi (e.g., [24,39,40,77,78]). However, unambiguously recognizing the taxonomic placement of Precambrian organic-walled microfossils can be difficult, due to the many morphological convergences observed between lineages (see [79] for review). Similarly, a taxonomic placement based on FTIR signals or chemistry alone would suffer from the many convergences observed in wall compositions between and within lineages (e.g., polyphyletic algae; [5]) and the modifications undergone during the diagenesis (e.g., fossilization products). Such recognition must therefore be coupled with morphological and ultrastructural analyses [24,79]. Nevertheless, using the proxies presented here, we can estimate the kerogen composition and possible precursors for the different microfossils. *Herisphaera arbovela* show a composition rich in aliphatic and oxygenated compounds. The spectral and chemometric characteristics of *Herisphaera* suggest an original composition similar to algaenan-like material. Algaenan is designating a group of biogeomolecules constituted of long aliphatic building block (22 to more than 40 carbon atoms; [5]) connected by ester and ether cross links, observed in numerous microalgae [5,20].

Germinosphaera alveolata show a very high aromatic contribution coupled with the presence of aliphatic chains of 18 carbons. This high aliphatic contribution is also explaining the medium Al/C═C value (0.17) despite the very high absorption for aromatic moieties. The clear absorption for carbonyl groups is suggesting a high oxygenated contribution. However, *G. alveolata* present the lowest C factor and C═O/C═C values. This very high aromatic intensity coupled with high aliphatic and oxygenated contribution and a low calculated Raman temperature suggests that the wall of *G. alveolata* was originally rich in aromatic compounds rather than resulting from carbonization. A high aromatic, high aliphatic composition associated with oxygenated moieties is known amongst micro-algae and protists [5,80].

Ourasphaira shows an oxygenated composition coupled with moderate length aliphatic chains (ca. 10 carbons). It presents the lowest aromaticity ratio for the three Grassy Bay taxa but an absence of clear absorption around 3050 cm^{-1} (CH stretching in aromatic rings and alkene groups), which suggests that unsaturated carbon compounds are less contributing to their original composition compared to the other Grassy Bay fossils. Thus, the strong intensity of the absorption band at 1592 cm^{-1} might also result from an increased contribution of other compounds absorbing in the interval 1650–1550 cm^{-1}, notably C═O stretching and N-moieties [50,51]. *Ourasphaira* was interpreted as a fungus based on the combination of morphological, ultrastructural characters and a chemical composition compatible with chitinous products [24] although doubts may subsist on this affinity [81]. Fungal cell walls are composed mainly of polysaccharides (up to 89% of the dry content; chitin and glucans), proteins (up to 20%; mostly glycoproteins) and subordinate lipids, minerals and pigments [82,83]. Such composition will lead to a higher contribution of sugars-protein fossilization products in their kerogen [6,56,57], as observed here.

Germinosphaera bispinosa is characterized by a moderate aliphatic

chain (ca. 9–10 carbons). Carboxyl and oxygenated compounds are also abundant as shown by the high C═O/C═C ratio and C factor. However, the relatively low Al/C═C ratio and A factor show the predominance of aromatic absorption over aliphatic. This is also indicated by the presence of the well-defined absorption band at 3044 cm^{-1}. Because they underwent the same thermal history as other Grassy Bay microfossils, the strong aromatic composition of *G. bispinosa* certainly reflect the higher contribution of aromatic compounds to its original composition. The very strong absorption observed at 1258 cm^{-1} (and shoulder at 1210 cm^{-1}) indicates the contribution of aromatic ethers and phenol [17,50].

An aromatic structure with oxygen containing groups is observed in sporopollenin material, a polymer of para-coumaric and ferulic acids [3,5,17]. This very resistant compound is found in the wall of pollens and spores but originated in micro-algae, where it is linked with resistance to environmental stress [5,84]. However, in sporopollenin, para-coumaric and ferulic acids are usually associated with highly aliphatic groups [3,5,17]. In the present case, the aliphatic contribution is moderate. It is possible that the microfossils were composed of a sporopollenin-like material but coupled with shorter aliphatic chains. However, in Grassy Bay, all studied microfossils present moderate aliphatic chain length composed of 9–10 carbons. This low aliphaticity may also result from the diagenetic degradation and aromatization of the material.

Finally, *Herisphaera triangula* presents low Al/C═C values, coupled with a well-defined absorption around 3050 cm^{-1}, indicating an aromatic contribution. Like other Grassy Bay specimens, their $R_{3/2}$ ratio illustrate the presence of moderate aliphatic chains (ca. 9–10 carbons). The microfossils also present a relatively low oxygenated content as revealed by their C═O/C═C ratio despite the presence of a well-defined absorption for C═O groups. We can also observe the presence of phenolic compound although in weaker intensity than for *Germinosphaera bispinosa*.

Studies have shown that the detection of highly aliphatic signatures in kerogen was certainly more complex than simple selective preservation of original biopolymers, with possible incorporation of external aliphatic polymers into the kerogen [85,86] or formation of aliphatic geopolymer during the diagenesis [87]. The presence of highly aliphatic signatures can be especially doubtful when it occurs in fossils for which the living counterparts were not producing such compounds [87,88]. In our material, *H. arbovela* and *G. alveolata* display FTIR signatures of long-chain aliphatic molecules (15–16 and 18 carbons, respectively). Although their original taxonomic affiliation is unclear, they could represent microalgae or other protists [39,40,77,79]; affinities compatible with the presence of such polymers (e.g., [5]). Their low Raman temperature estimates (ca. 125 °C for *H. arbovela* and ca. 140 °C for *G. alveolata*) are also compatible with selective preservation of long aliphatic chains. Therefore, despite not being completely excludable, the highly aliphatic signature of *H. arbovela* and *G. alveolata* are unlikely to result from external or geo-formed aliphatic compounds. However, further interpretation over their living molecular composition, especially algaenan for *H. arbovela*, should be consider with caution (hence the use of "algaenan-like" above).

6. Conclusions

The present approach, applied here on 5 morphospecies of Proterozoic eukaryotes can easily be used in complement of, or in absence of possible, bands-by-bands assignments, often difficult due to the complex molecular structure of kerogen. Using a combination of proxies, this routine permitted, not only a description of kerogen type and composition for each of these microfossils, but also the discrimination between biological and maturation signals (carbonization), further supported using Raman geothermometry. Although applicable with any FTIR instrument, the use of SR-FTIR provides here a higher spatial resolution that allows the possibility to select spectra of reference within the microfossils, attenuating the biases caused by spectral distortion, preservation heterogeneities or acquisition artefacts (e.g., organic debris on the wall surface). Such technique is still scarcely applied on Precambrian microfossils and mostly on fossils in rock thin sections. It yields here interesting new results on extracted organic-walled vesicular microfossils of unknown or unclear identity. This investigation demonstrates the interest of combining qualitative and semi-quantitative approaches of FTIR spectroscopy for a meaningful characterization of the kerogen of Precambrian organic microfossils.

Funding

This work was supported by the FRS-FNRS CR UPRISE (C.C.L, Belgium) and CR PROMESS (MC.S, Belgium); two Soleil Synchrotron CALIPSOplus grants (C.C.L and MC.S, EU); the Agouron Institute (US) project "Unraveling the Record of Proterozoic Eukaryotic Evolution in the Canadian Arctic" (E.J.J; C.C.L); the ERC Stg ELiTE FP7/308074 (E.J.J, EU); the FRS-FNRS-FWO EOS ET-HOME grant 30442502 (E.J.J, Belgium) and the Belspo BRAIN PORTAL project (E.J.J, Belgium). C.C.L is currently supported by The Royal Society (UK) and the WBI (Belgium).

CRediT authorship contribution statement

Corentin C. Loron: Conceptualization, Methodology, Investigation, Formal analysis, Writing – original draft. **Marie Catherine Sforna**: Investigation, Visualization, Formal analysis, Writing – review & editing. **Ferenc Borondics**: Investigation, Resources, Validation, Writing – review & editing. **Christophe Sandt**: Investigation, Resources, Validation, Writing – review & editing. **Emmanuelle J. Javaux**: Supervision, Conceptualization, Writing – original draft.

Declaration of Competing Interest

The authors declare that they have no known competing financial interests or personal relationships that could have appeared to influence the work reported in this paper.

Data availability

Data will be made available on request.

Acknowledgments

R.H. Rainbird, E.C. Turner, T. Skulski, G.P. Halverson and Geological Survey of Canada's Geomapping for Energy and Minerals Program are thanked for the fieldwork logistics and help with sample collection. M. Giraldo and A. Lambion (U. Liege) are thanked for the sample preparation. Synchrotron Soleil (Gif-sur-Yvette, France) is thanked for providing synchrotron radiation beamtime at SMIS beamline (proposal 190522; C.C.L, E.J.J, MC.S).

Appendix A. Supporting information

Supplementary data associated with this article can be found in the online version at doi:10.1016/j.vibspec.2022.103476.

References

[1] Konhauser, K.O., John Wiley & Sons, 2009.
[2] Briggs, D.E.G.Palaios, 1995: 539–550.
[3] R.B.L. Yule, J. Marshall, Org. Geochem. 31 (9) (2000) 859–870.
[4] Killops, S.D., and Killops V.J. John Wiley & Sons, 2013.
[5] J.W. de Leeuw, G.J.M. Versteegh, P.F. van Bergen, Plant Ecol. 182 (1) (2006) 209–233.
[6] J. Wiemann, J.M. Crawford, D.E. Briggs, Sci. Adv. 6 (28) (2020) eaba6883.
[7] B. Durand, G. Nicaise, Editions technip,, 1980.
[8] C.P. Marshall, E.J. Javaux, A.H. Knoll, M.R. Walter, Precambrian Res. 138 (3-4) (2005) 208–224.
[9] A. Olcott Marshall, C.P. Marshall, Palaeontology 58 (2) (2015) 201–211.

[10] P.C. Painter, R.W. Snyder, M. Starsinic, M.M. Coleman, D.W. Kuehn, A. Davis, Appl. Spectrosc. 35 (5) (1981) 475–485.
[11] H. Ganz, W. Kalkreuth, Fuel 66 (5) (1987) 708–711.
[12] R. Lin, G.P. Ritz, Org. Geochem. 20 (6) (1993) 695–706.
[13] Y. Guo, R.M. Bustin, Int. J. Coal Geol. 36 (3–4) (1998) 259–275.
[14] G.P. Lis, M. Mastalerz, A. Schimmelmann, M.D. Lewan, B.A. Stankiewicz, Org. Geochem. 36 (11) (2005) 1533–1552.
[15] Y. Zeng, C. Wu, Fuel 86 (7–8) (2007) 1192–1200.
[16] Rui Lin, G.Patrick Ritz, "Reflectance FT-IR microspectroscopy of fossil algae contained in organic-rich shales.", Appl. Spectrosc. 47 (3) (1993) 265–271.
[17] P. Steemans, K. Lepot, C.P. Marshall, A. Le Hérissé, E.J. Javaux, Rev. Palaeobot. Palynol. 162 (4) (2010) 577–590.
[18] J.A. D'Angelo, E.L. Zodrow, A. Camargo, Org. Geochem. 41 (12) (2010) 1312–1325.
[19] J.A. D'Angelo, E.L. Zodrow, Org. Geochem. 42 (9) (2011) 1039–1054.
[20] S. Dutta, C. Hartkopf-Fröder, K. Witte, R. Brocke, U. Mann, Int. J. Coal Geol. 115 (2013) 13–23.
[21] E.J. Javaux, A.H. Knoll, C.P. Marshall, M.R. Walter, Third Eur. Workshop Exo-Astrobiol. Vol. 545 (2004).
[22] E.J. Javaux, C.P. Marshal, Rev. Palaeobot. Palynol. 139 (1–4) (2006) 1–15.
[23] C.P. Marshall, E.A. Carter, S. Leuko, E.J. Javaux, Vib. Spectrosc. 41 (2) (2006) 182–189.
[24] C.C. Loron, C. François, R.H. Rainbird, E.C. Turner, S. Borensztajn, E.J. Javaux, Nature 570 (7760) (2019) 232–235.
[25] S. Bonneville, F. Delpomdor, A. Préat, C. Chevalier, T. Araki, M. Kazemian, L. G. Benning, Sci. Adv. 6 (4) (2020) eaax7599.
[26] M. Igisu, T. Komiya, M. Kawashima, S. Nakashima, Y. Ueno, J. Han, K. Takai, Gondwana Res. 25 (3) (2014) 1120–1138.
[27] M. Igisu, T. Komiya, Y. Ikemoto, Y. Geng, H. Uehara, Geochem. J. 51 (6) (2017) 589–594.
[28] Igisu, M., Komiya, T., Awramik, S.M., Ikemoto, Y., Geng, Y., Uehara, H., & Takai, K. Precambrian Research 373 (2022): 106628.
[29] Y. Cornet, C. François, P. Compère, Y. Callec, S. Roberty, J.C. Plumier, E.J. Javaux, Precambrian Res. 332 (2019), 105410.
[30] K. Hickman-Lewis, F. Westall, B. Cavalazzi, Palaeontology 63 (6) (2020) 1007–1033.
[31] M. Igisu, T. Komiya, S.M. Awramik, Y. Ikemoto, Y. Geng, H. Uehara, K. Takai, Isl. Arc 28 (5) (2019), e12310.
[32] J.L. Bishop, C. Koeberl, C. Kralik, H. Fröschl, P.A. Enolert, D.W. Andersen, R. A. Wharton Jr, Geochim. Et. Cosmochim. Acta 60 (5) (1996) 765–785.
[33] Kristin N. Alstadt, R.Katti Dinesh, Kalpana S. Katti, Spectrochim. Acta Part A: Mol. Biomol. Spectrosc. 89 (2012) 105–113.
[34] M. Vandenbroucke, C. Largeau, Org. Geochem. 38 (5) (2007) 719–833.
[35] Q. Tang, K. Pang, G. Li, L. Chen, X. Yuan, S. Xiao, Gondwana Res. 97 (2021) 22–33.
[36] E.J. Javaux, A.H. Knoll, M.R. Walter, Geobiology 2 (3) (2004) 121–132.
[37] A.H. Knoll, E.J. Javaux, D. Hewitt, P. Cohen, Philos. Trans. R. Soc. B: Biol. Sci. 361 (1470) (2006) 1023–1038.
[38] Phoebe A. Cohen, A.Macdonald Francis, Paleobiology 41 (4) (2015) 610–632.
[39] C.C. Loron, R.H. Rainbird, E.C. Turner, J.W. Greenman, E.J. Javaux, Precambrian Res. 321 (2019) 349–374.
[40] C.C. Loron, G.P. Halverson, R.H. Rainbird, T. Skulski, E.C. Turner, E.J. Javaux, J. Paleontol. 95 (6) (2021) 1113–1137.
[41] E.J. Javaux, A.H. Knoll, M.R. Walter, Orig. Life Evol. Biosphere 33 (1) (2003) 75–94.
[42] E.J. Javaux, A.H. Knoll, M.R. Walter, Nature 412 (6842) (2001) 66–69.
[43] Nicholas J. Butterfield, Palaeontology 58 (1) (2015) 5–17.
[44] R.H. Rainbird, C.W. Jefferson, G.M. Young, Geol. Soc. Am. Bull. 108 (4) (1996) 454–470.
[45] N.M. Rayner, R.H. Rainbird, Open File, 7419, Geological Survey of Canada,, 2013, pp. 10–4095.
[46] D. van Acken, D. Thomson, R.H. Rainbird, R.A. Creaser, Precambrian Res. 236 (2013) 124–131.
[47] J.W. Greenman, Robert Howard Rainbird, Geological Survey of Canada,, 2018.
[48] R.H. Rainbird, A.D. Rooney, R.A. Creaser, T. Skulski, Earth Planet. Sci. Lett. 548 (2020), 116492.
[49] Grey, K. Geological Survey of western Australia (1999).
[50] J. Coates, in: Chemistry R.A. Meyers (Ed.), Encyclopedia of Analytical, 2000, pp. 10815–10837.
[51] Silverstein, R.M., Webster, F.X., Kiemle, D., Bryce, D.L. John Wiley & Sons (Eds), 2014: 464 pp.
[52] B.K. Baludikay, C. François, M.C. Sforna, J. Beghin, Y. Cornet, J.Y. Storme, E. J. Javaux, Int. J. Coal Geol. 191 (2018) 80–94.
[53] S. Wang, P.R. Griffiths, Fuel 64 (2) (1985) 229–236.
[54] M. Igisu, Y. Ueno, M. Shimojima, S. Nakashima, S.M. Awramik, H. Ohta, S. Maruyama, Precambrian Res. 173 (1–4) (2009) 19–26.
[55] M. Igisu, K. Takai, Y. Ueno, M. Nishizawa, T. Nunoura, M. Hirai, Y. Isozaki, Environ. Microbiol. Rep. 4 (1) (2012) 42–49.
[56] G.F. Mohsin, F.J. Schmitt, C. Kanzler, J.D. Epping, S. Flemig, A. Hornemann, Food Chem. 245 (2018) 761–767.
[57] V.E. McCoy, J. Wiemann, J.C. Lamsdell, C.D. Whalen, S. Lidgard, P. Mayer, D. E. Briggs, Geobiology 18 (5) (2020) 560–565.
[58] G. Hantal, L. Brochard, M.N. Dias Soeiro Cordeiro, F.J. Ulm, R.J.M. Pellenq, J. Phys. Chem. C. 118 (5) (2014) 2429–2438.
[59] S. McMahon, R.P. Anderson, E.E. Saupe, D.E. Briggs, Geology 44 (10) (2016) 867–870.
[60] R.P. Anderson, N.J. Tosca, R.R. Gaines, N.M. Koch, D.E. Briggs, Geology 46 (4) (2018) 347–350.
[61] Bernard P. Tissot, Dietrich H. Welte, Springer,, Berlin, Heidelberg, 1984, pp. 69–73.
[62] A. Lahfid, O. Beyssac, E. Deville, F. Negro, C. Chopin, B. Goffé, Terra Nova 22 (2010) 354–360.
[63] Y. Kouketsu, T. Mizukami, H. Mori, S. Endo, M. Aoya, H. Hara, S. Wallis, Isl. Arc 23 (1) (2014) 33–50.
[64] J. Mathieu, D.J. Kontak, E.C. Turner, Geofluids 13 (6) (2013) 559–578.
[65] K. Pang, Q. Tang, C. Wu, G. Li, L. Chen, B. Wan, S. Xiao, Precambrian Res 346 (2020), 105818.
[66] D.M. Hudgins, S.A. Sandford, J. Phys. Chem. A 102 (2) (1998) 329–343.
[67] D.M. Hudgins, S.A. Sandford, J. Phys. Chem. A 102 (2) (1998) 344–352.
[68] M. Kacurakova, P. Capek, V. Sasinkova, N. Wellner, A. Ebringerova, Carbohydr. Polym. 43 (2) (2000) 195–203.
[69] Ritsuko Hori, Junji Sugiyama, "A combined FT-IR microscopy and principal component analysis on softwood cell walls.", Carbohydr. Polym. 52 (4) (2003) 449–453.
[70] V. Shapaval, T. Møretrø, H.P. Suso, A.W. Åsli, J. Schmitt, D. Lillehaug, A. Kohler, J. Biophotonics 3 (8–9) (2010) 512–521.
[71] X. Liu, C.M. Renard, S. Bureau, C. Le Bourvellec, Carbohydr. Polym. 262 (2021), 117935.
[72] E. Wiercigroch, E. Szafraniec, K. Czamara, M.Z. Pacia, K. Majzner, K. Kochan, K. Malek, Spectrochim. Acta Part A: Mol. Biomol. Spectrosc. 185 (2017) 317–335.
[73] M.P. Fuller, I.M. Hamadeh, P.R. Griffiths, D.E. Lowenhaupt, Fuel 61 (1982) 529–536.
[74] M. Mastalerz, R.M. Bustin, Fuel 74 (4) (1995) 536–542.
[75] M.J. Iglesias, A. Jimenez, F. Laggoun-Defarge, I. Suarez-Ruiz, Energy Fuels 9 (3) (1995) 458–466.
[76] J. Ibarra, E. Munoz, R. Moliner, Org. Geochem. 24 (1996) 725–735.
[77] L. Miao, M. Moczydłowska, S. Zhu, M. Zhu, Precambrian Res. 321 (2019) 172–198.
[78] C.C. Loron, M. Moczydłowska, Palynology 42 (2) (2018) 220–254.
[79] E.J. Javaux, Nature 572 (7770) (2019) 451–460.
[80] A.R. Hemsley, P.J. Barrie, W.G. Chaloner, NERC Spec. Publ. 94 (1) (1994) 15–19.
[81] M.L. Berbee, C. Strullu-Derrien, P.M. Delaux, et al., Nat. Rev. Microbiol. 18 (2020) 717–730.
[82] Ruiz-Herrera, J. CRC press, 1991.
[83] V. Mohaček-Grošev, R. Božac, G.J. Puppels, Spectrochim. Acta Part A: Mol. Biomol. Spectrosc. 57 (14) (2001) 2815–2829.
[84] X. He, D. Junbiao, Q. Wu, Front. Microbiol. 7 (2016) 1047.
[85] G.J. Versteegh, P. Blokker, Phycol. Res. 52 (4) (2004) 325–339.
[86] R.B. Kodner, R.E. Summons, A.H. Knoll, Org. Geochem. 40 (8) (2009) 854–862.
[87] M.M. Kuypers, P. Blokker, E.C. Hopmans, H. Kinkel, R.D. Pancost, S. Schouten, J.S. S. Damsté, Palaeogeogr., Palaeoclimatol., Palaeoecol. 185 (1–2) (2002) 211–234.
[88] N.S. Gupta, M.E. Collinson, D.E. Briggs, R.P. Evershed, R.D. Pancost, Paleobiology 32 (3) (2006) 432–449.